Calculation of Vibrational Spectra of Linear Tetrapyrroles. 3. Hydrogen-Bonded Hexamethylpyrromethene Dimers

Maria-Andrea Mroginski,[†,‡] Károly Németh,[†] Tanja Bauschlicher,[†] Werner Klotzbücher,[†] Richard Goddard,[§] Oliver Heinemann,[§] Peter Hildebrandt,*[,‡] and Franz Mark*[,†]

Max-Volmer-Laboratorium, Institut für Chemie, Technische Universität Berlin, Sekr. PC 14, Strasse des 17 Juni 135, D-10623 Berlin, Germany, Max-Planck-Institut für Bioanorganische Chemie, Postfach 101365, D-45413 Mülheim an der Ruhr, Germany, and Max-Planck-Institut für Kohlenforschung, Kaiser-Wilhelm-Platz 1, D-45470 Mülheim an der Ruhr, Germany

Received: September 16, 2004; In Final Form: December 19, 2004

The structure and vibrational spectra of hexamethylpyrromethene (HMPM) have been investigated by X-ray crystallography, IR and Raman spectroscopies, and density functional theory calculations. HMPM crystallizes in the form of dimers, which are held together by bifurcated N−H(···N)$_2$ hydrogen bonds, involving one intramolecular and one intermolecular N−H···N interaction. The monomers are essentially planar, and the mean planes of the monomers lie approximately perpendicular to one another, so that the four N atoms in the dimer form a distorted tetrahedron. The structure of the HMPM dimer is well-reproduced by B3LYP/6-31G* calculations. A comparison of the calculated geometry of the dimer with that of the monomer reveals only small changes in the N−H···N entity and the methine bridge angles upon dimerization. These are a result of weakening of the intramolecular N−H···N hydrogen bond and the formation of a more linear N−H···N intermolecular hydrogen bond. Using an empirical relation between the shift of the N−H stretching frequency of pyrrole and the enthalpy of adduct formation with bases [Nozari, M. S.; Drago, R. S. *J. Am. Chem. Soc.* **1970**, *92*, 7086−7090], estimates of the strength of the intra- and intermolecular hydrogen bonds are obtained. IR and Raman spectroscopies of HMPM and its isotopomers deuterated at the pyrrolic nitrogen atom and at the methine bridge reveal that the molecule is monomeric in nonpolar organic solvents but dimeric in a solid Ar matrix and in KBr pellets. The matrix IR spectra show a splitting of vibrational modes for the dimer, particularly those involving the N−H coordinates. Due to intrinsic deficiencies of the B3LYP/6-31G* approximation, a satisfactory reproduction of these modes of the monomeric and dimeric HMPM requires specific adjustments of the NH scaling factors for the calculated force constants and, in the case of the NH out-of-plane modes of HMPM dimers, also of intra- and intermolecular coupling constants. This parametrization does not significantly affect the other calculated modes, which in general reveal a very good agreement with the experimental data.

Introduction

Despite the methodological progress that has been achieved in NMR spectroscopy and X-ray crystallography in recent years, vibrational spectroscopy remains an indispensable tool for elucidating structure−dynamics−function relationships of cofactor−protein complexes, since it can provide important information about the hydrogen bond interactions that largely determine the molecular structure and reactivity of the prosthetic group. Continuing our previous studies on model compounds for the tetrapyrrole chromophore in the photoreceptor phytochrome (for recent reviews see refs 1-3), we address here hexamethylpyrromethene (HMPM; Chart 1).[4] The molecule is interesting for a number of reasons: First, it is a mimic for the central dipyrrole unit of phytochromobilin.[5] Second, it can form both intra- and intermolecular hydrogen bonds involving the N−H group, interactions which are thought to play a role in the chromophore−protein complex in phytochrome. Third, it represents an instructive model system for elucidating the effect of hydrogen bond interactions on the vibrational spectra of substituted pyrrole and pyrrolenine ring systems. In addition, early on in our investigations we realized that whereas HMPM occurs as a monomer in nonpolar organic solvents, in the solid it occurs as a dimer, enabling us to study in detail the effect of association on the vibration spectra.

CHART 1

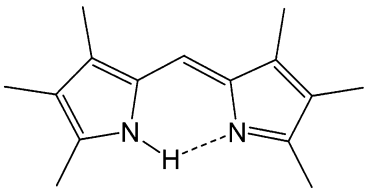

hexamethylpyrromethene (HMPM)

In a recent work,[4] we analyzed the resonance Raman (RR) spectrum of monomeric HMPM. However, Raman spectroscopy applied to this problem has the disadvantage that most of the modes that include coordinates of the N−H group exhibit only

* Corresponding authors. (P.H.) Telephone: +493031421419. Fax: +0493031421122. E-mail: Hildebrandt@chem.tu-berlin.de. (F.M.) Telephone: +492083063697. Fax: +492083063951. E-mail: mark@mpi-muelheim.mpg.de.

[†] Max-Planck-Institut für Bioanorganische Chemie.

[‡] Technische Universität Berlin.

[§] Max-Planck-Institut für Kohlenforschung.

10.1021/jp045805y CCC: $30.25
Published on Web 02/22/2005

weak RR intensities. In this respect, IR spectroscopy is the more appropriate technique, and hence it was employed in the present study. In particular, by using conventional IR spectroscopy together with argon matrix IR spectroscopy, it was possible to study both HMPM monomers and dimers to determine the intra- and intermolecular hydrogen bond interactions. How these can be taken into account in the quantum chemical calculation of vibrational spectra is a prerequisite for determining the phytochromobilin structure in the various states of the photoreceptor.[6] In the absence of hydrogen bonds, scaled force fields obtained from density functional theory (DFT) have already been shown to be an efficient approach for predicting the normal modes of model compounds with an accuracy of ca. 11 cm^{-1}.[7] For hydrogen bonded systems, however, deficiencies of DFT are known.[8] An appropriate choice of scaling factors may at least in part compensate these drawbacks, but up to now a systematic survey has not yet been carried out.

In this combined experimental and theoretical work, we analyze the structure of HMPM monomers and dimers and their vibrational spectra, with a view to determining the scaling factors for the theoretical calculation of internal coordinates of the N−H groups in N−H···N systems involving the pyrrole group and discuss the possibilities and limitations of the transferability of these scaling factors to other hydrogen bonded systems.

Materials and Methods

(1) Syntheses. HMPM was prepared and purified as described elsewhere.[4] N-deuterated HMPM (HMPM-ND) was obtained by reacting the nondeuterated compound (HMPM-D_0) with deuteriotrifluoroacetic acid and converting the salt into the free base with deuterioammonia. A 30 mg amount of HMPM-D_0 was dissolved at ambient temperature in 3 mL of CF_3COOD, and the acid was evaporated after 30 min at 30 °C under reduced pressure. This process was repeated three times. The residual was dissolved in a 100 mL flask in a mixture of 2 mL of CH_3OD, 2 mL of D_2O, and 10 mL of CH_2Cl_2, and the solution was exposed twice to gaseous ND_3 under shaking. After removal of the aqueous phase, the organic phase was washed three times with 2 mL of D_2O. Upon addition of CH_3OD, N-deuterated HMPM was obtained in crystalline form. According to the NMR spectrum in $CDCl_3$, complete N-deuteration was achieved by this procedure; however, D/H reexchange seems to occur very rapidly even with moisture in the air.

HMPM, deuterated at the methine bridge (3,3′,4,4′,5,5′-hexamethyl-*ms*-deuteriopyrromethene,[9] (HMPM-CD), was synthesized via a condensation reaction of 2-(ethoxycarbonyl)-3,4,5-trimethylpyrrole (ETP) with dideuterioformic acid. Published procedures[10,11] have been modified in order to allow for a small-scale synthesis and for the isolation of an intermediate, the hydrochloride of HMPM, which we needed for further spectroscopic studies. A 200 mg amount of ETP, synthesized according to ref 4, was dissolved in 1 mL of DCOOD (98% isotopically pure). After addition of 0.5 mL of concentrated HCl, the solution was heated for 8 h at 100 °C under Ar gas protection in a Schlenk tube with reflux condenser. During heating, a yellow solid precipitated from the dark red solution. The reaction mixture was left at ambient temperature overnight, and the yellow solid was filtered off and washed with diethyl ether and formic acid. Upon treatment of the mother liquor with diluted (1:1) aqueous ammonia solution, additional yellow solid precipitated. The combined products were dissolved in $CHCl_3$ and shaken twice with diluted (1:1) aqueous ammonia solution. After removal of the solvent and crystallization in ethanol, 0.028 g of HMPM-CD was obtained in the form of black prisms with mp of 153 °C (decomposition starting at 130 °C).

(2) X-ray Crystal Data for HMPM. HMPM ($C_{15}H_{20}N_2$, M_r = 228.33) was crystallized from acetone solution to yield triclinic crystals [0.25 × 0.28 × 0.67 mm^3; space group, $P\bar{1}$, no. 2; a = 8.4100(5) Å, b = 12.0341(5) Å, and c = 13.4913(10) Å; α = 88.641(4)°, β = 76.120(5)°, and γ = 87.688(4)°; V = 1324.3(1) $Å^3$; T = 293 K; Z = 4; ρ_{calcd} = 1.145 g cm^{-3}; $F(000)$ = 496]. Data were collected with a Nonius CAD-4 diffractometer [λ(Cu Kα) = 1.541 78 Å; μ = 0.516 mm^{-1}; 5690 measured and 5449 independent reflections (R_{int} = 0.014), 4728 with $I > 2\sigma(I)$; θ_{max} = 75.04°; no absorption correction]. Structure was solved by direct methods and refined by least-squares methods[12] {Chebychev weights on F_o^2 to R_1 = 0.0583 [$I > 2\sigma(I)$], R_{w2} = 0.1789 (all data), 327 parameters; H1 and H3 (on N1 and N3) isotropic adp's, otherwise H atoms riding; Δ/σ < 0.001; S = 1.045; residual electron density, 0.270/−0.265 e $Å^{-3}$}.

(3) IR Investigations. Matrix isolation IR spectra were obtained with a setup described previously,[13,14] which is characterized by a quartz crystal microbalance mounted on the sample window. The sample chamber equipped with NaCl windows was linked to a Perkin-Elmer 1760 FTIR spectrometer. HMPM was evaporated from a heatable glass inlet source. At a heating temperature of 70−80 °C, a guest−host ratio of approximately 1−2 to 10 000 was achieved. In the case of HMPM-ND, unavoidable traces of water caused a substantial D/H reexchange after introducing the deuterated HMPM into the sample chamber.

IR spectra of HMPM dissolved in organic solvents (cyclohexane, CCl_4, CD_2Cl_2; concentrations, ∼10 mmol·L^{-1}) and in KBr were recorded with an IFS 66 interferometer (Bruker) using a resolution of 4 cm^{-1}. H/D exchange at the pyrrole nitrogen was achieved by saturating the organic solvents with D_2O.

(4) Theoretical Calculations. DFT calculations with the B3LYP functional[15] and the 6-31G* basis set[16] were carried out as described previously.[4] The force fields were scaled according to

$$(F_{ij})^{\sigma} = \sqrt{\sigma_i}(F_{ij})\sqrt{\sigma_j} \qquad (1)$$

where $(F_{ij})^{\sigma}$ and F_{ij} are the respective scaled and unscaled force constants of the internal coordinates i and j.[17] A previously determined set of global scaling factors σ_i was used[7] except for the internal coordinates of the N−H group which have been further refined in this work.

Results and Discussion

(1) Crystal Structure and Calculated Structures. Summarized in Figure 1are the results of the crystal structure analysis of HMPM, which reveal that the molecule exists as a dimer in the crystal. The dimer adopts an interesting configuration in which the mean planes through the two monomeric molecules lie approximately perpendicular to one another (87.96(2)°), so that the four N atoms making up the dimer form an approximate tetrahedron. The two pyrrolic H atoms in the dimer were localized in a difference Fourier synthesis calculated using the remaining atoms in the structure, and their atomic positions refined satisfactorily (U_{H1} = 0.09(1) $Å^2$, U_{H3} = 0.11(1) $Å^2$). They are found to be attached solely to N1 (H1) and N3 (H3), and the dimer is held together by bifurcated N−H(···N)$_2$ hydrogen bonds,[18] in which H1 is bonded to N2 and N4, and H3 to N2 and N4. As a result, the bonds in the remainder of the molecule are strongly localized (cf. C1−C2, 1.388(2) Å; C8−C9, 1.450(2) Å (see Table 1)), and the dimer possesses an approximate (noncrystallographic) 2-fold axis passing through

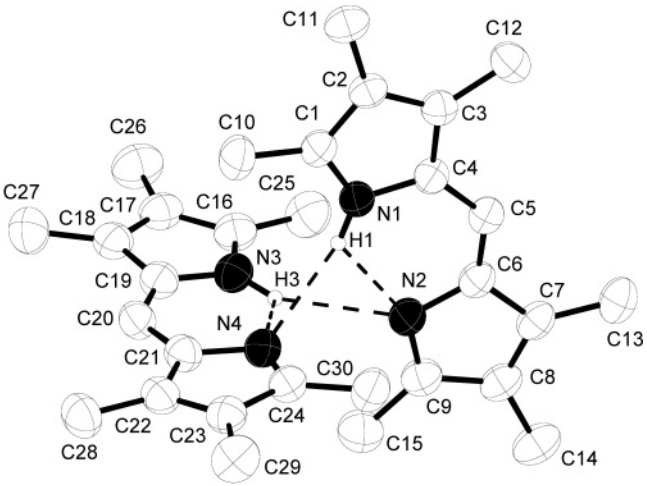

Figure 1. Structure of HMPM dimer in the crystal. An approximate 2-fold axis passes through an axis defined by the midpoint of N1 and N3 and the midpoint of N2 and N4. Selected distances (Å), angles (deg), and dihedral angles (deg): N1−H1, 0.90(3); N3−H3, 0.92(3); N1···N2, 2.902(2); N1···N3, 3.436(2); N1···N4, 3.120(2); N2···N3, 3.194(2); N2···N4, 3.275(2); N3···N4, 2.872(2); H1···N2, 2.32(3); H1···N3, 2.78(3); H1···N4, 2.34(3); H3···N1, 3.02(3); H3···N2, 2.35(3); H3···N4, 2.36(2); mean plane(N1,N2,C1−C15)/mean plane(N3,N4,C16−C30), 87.96(2).

an axis defined by the midpoint of N1 and N3 and the midpoint of N2 and N4. Since the two rings of HMPM are not equivalent, such dimers are chiral and each elementary cell in fact contains both dimers of the chiral pair.

It is interesting to note that despite the large variation in the N···N distances within the N tetrahedron, the intramolecular H···N hydrogen bond distances (H1···N2, 2.32(3) Å; H3···N4, 2.36(3) Å) are not significantly different from the intermolecular H···N hydrogen bond distances (H1···N4, 2.34(3) Å; H3···N2, 2.35(2) Å). This similarity is, however, not reflected in the N−H···N angles, where the intramolecular N−H···N angles (mean, 119(4)°) are markedly smaller than the intermolecular N−H···N angles (mean, 149(6)°), indicating that the intermolecular N−H···N bonds are more linear. If the apparent N−H bond shortening inherent to the X-ray method[18] is taken into account, the differences in the angles are expected to become larger.

The geometry of the dimeric HMPM was optimized on the B3LYP/6-31G* level, taking the crystal structure data as initial parameters. In the converged structure, the dimer displays exact C_2 point symmetry. The monomeric units are slightly distorted along the methine bridge due to different interactions between the pyrrole rings of unit A and unit B and the pyrrolenine rings of unit A and unit B. In the crystal, the deviations from planarity are somewhat higher (plane(N1,C1−C4)/plane(N2,C6−C9), 3.46°; plane(N3,C16−C19)/plane(N4,C21−C24), 8.10°), which as well as the bond length and bond angle differences between the monomeric entities can be attributed to effects of the crystal packing and consequently result in a slight deviation from the ideal C_2 point symmetry. Despite these differences, the calculated bond lengths and bond angles agree very well with the experimental data with standard deviations of 0.007 Å and 0.8°, respectively (Table 1). The tetrahedral arrangement of the four nitrogens is also reproduced by the calculations, although the intramolecular and intermolecular N···N distances are slightly overestimated.

The excellent performance of the DFT calculations in calculating the structure of the HMPM dimer is in line with previous findings[19] and confirms the view that comparably reliable results are obtained for the geometry optimization of the HMPM monomer, for which no experimental data are currently available. In monomeric HMPM, the overall geometry remains nearly unchanged compared to the monomeric entities of the dimer. The standard deviation for the bond lengths is 0.001 Å with the largest deviation of 0.004 Å. For the bond angles, the standard deviation is 0.8°, and the differences between the monomer and dimer do not exceed |0.7|°, except for the methine bridge bond angles (+2.6° for C3−C4−C5 and

TABLE 1: Selected Experimental and Calculated Bond Lengths, Bond Angles, and Torsion Angles of Dimeric HMPM[a]

	X-ray		
	unit A N1C1···N2	unit B N3C16···N4	calcd
	Bond Lengths (Å)		
C2C1	1.388	1.400	1.402
C3C2	1.406	1.394	1.413
C4C3	1.406	1.417	1.411
C5C4	1.412	1.409	1.417
C6C5	1.372	1.374	1.374
C7C6	1.454	1.450	1.457
C8C7	1.361	1.368	1.374
C9C8	1.450	1.443	1.460
C10C1	1.486	1.487	1.495
C11C2	1.493	1.497	1.501
C12C3	1.495	1.490	1.499
C13C7	1.490	1.488	1.500
C14C8	1.494	1.496	1.499
C15C9	1.487	1.493	1.498
N1C1	1.353	1.350	1.361
N1C4	1.381	1.383	1.388
N2C6	1.402	1.399	1.402
N2C9	1.319	1.317	1.319
N1H1	0.90	0.92	1.021
N2···H1	2.32	2.36	2.314
N4···H1	2.34	2.35	2.349
N3···H1	2.78	3.02	3.013
N1···N2	2.902	2.872	2.937
N1···N4	3.120	3.194	3.263
N1···N3	3.436		3.642
N2···N4	3.275		3.392
	Bond Angles (deg)		
C1C2C3	106.96	107.37	107.22
C2C3C4	107.54	107.27	107.55
C3C4C5	128.92	128.75	128.33
C4C5C6	128.54	128.11	128.95
C5C6C7	127.01	128.05	126.48
C6C7C8	106.15	105.90	105.72
C7C8C9	106.23	106.40	105.92
C2C1C10	128.90	129.69	130.13
C1C2C11	124.90	126.01	127.17
C2C3C12	126.16	125.98	125.25
C6C7C13	126.63	126.74	125.54
C7C8C14	127.75	128.02	129.42
C8C9C15	126.14	126.38	125.29
C2C1N1	108.95	108.79	108.27
C3C4N1	106.90	107.00	106.81
C1N1C4	109.65	109.57	110.15
C5C6N2	123.50	122.53	123.35
C8C9N2	112.30	112.03	112.53
C6N2C9	105.84	106.27	105.66
N1H1···N2	121.81	115.49	118.20
N1H1···N3	130.98	109.51	148.45
N1H1···N4	144.80	152.45	120.75

	X-ray		calcd
	Torsion Angles (deg)		
N1C4C5C6	2.45	6.17	2.89
C4C5C6N2	1.37	2.61	1.83

[a] The numbering of atoms refers to Figure 1; the geometry was optimized at the B3LYP/6-31G* level by imposing C_2 symmetry.

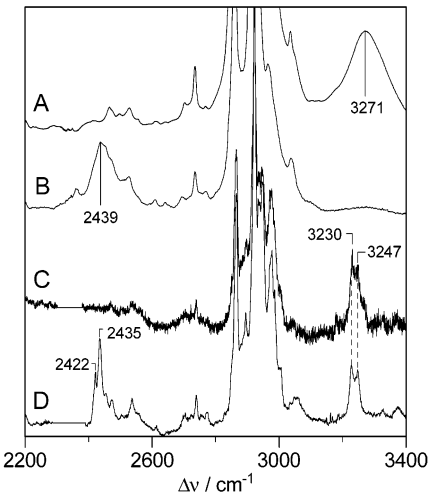

Figure 2. Experimental IR spectra of HMPM in the N−H/N−D stretching region: A, HMPM-D_0 monomers in CCl_4 solution; B, HMPM-ND monomers in CCl_4 solution; C, HMPM-D_0 dimers in Ar matrix; D, HMPM-ND dimers in Ar matrix.

−2.3° for C4−C5−C6). This structural alteration corresponds to a closer proximity of the two nitrogens (2.777 Å) in the monomer compared to the dimer (2.937 Å). These changes reflect a decrease in the strength of the intramolecular hydrogen bond in the dimer. Correspondingly, the calculated length of the intramolecular hydrogen bond is distinctly shorter in the monomer (2.027 Å) than that in the dimer (2.314 Å).

(2) Monomer−Dimer Equilibrium. The IR spectrum of HMPM-D_0 dissolved in CCl_4 displays a broad band at 3271 cm^{-1} (Figure 2A) which is slightly lower in frequency than the band reported previously (3281 cm^{-1}).[20,21] It can be unambiguously assigned to the N−H stretching, since it is replaced by a band at 2439 cm^{-1} in HMPM-ND (Figure 2B). The frequency of the N−H stretching of HMPM-D_0 is distinctly lower than the frequencies found for non-hydrogen-bonded pyrroles, such as 2,3,4-trimethylpyrrole, for which a value of 3490 cm^{-1} has been observed.[22] Hence, the frequency lowering can be attributed to the effect of hydrogen bond formation. For this band of HMPM-D_0 we and other authors have not found any concentration-dependent frequency changes in nonpolar organic solvents, such as CCl_4.[20] Instead, the IR band of the N−H stretching displays a linear Lambert−Beer behavior from 2 to 23 mmol·L^{-1}, ruling out dimerization of HMPM in this concentration range. Also for the related dipyrrole 3,3′,5,5′-tetramethyl,-4,4′-dicarbethoxypyrromethene, molecular weight measurements in $CHCl_3$ solution revealed no indication of association up to a concentration of 0.1 mol·L^{-1}.[23] Thus, it can be safely concluded that the IR spectra obtained from nonpolar organic solvents (Figure 2A,B) refer to monomeric HMPM, and the downshift of the N−H stretching frequency by 219 cm^{-1} relative to the frequency of non-hydrogen-bonded pyrroles originates from the intramolecular hydrogen bond in HMPM.

For hydrogen bonded adducts of pyrrole with hydrogen acceptors, Nozari and Drago[24] found a linear relationship between the association enthalpy at 298 K in CCl_4 solution and the shift of the N−H stretching frequency of a non-hydrogen-bonded pyrrole relative to that of the adduct. This empirical relationship will be adopted here to estimate the enthalpy of formation for the intramolecular hydrogen bond in HMPM, $\Delta H^{HB}_{298,mon}$, according to

$$\Delta H^{HB}_{298,mon} = -[a\cdot(\nu_0 - \nu_{mon}) + b] = -[a\cdot\Delta\nu_{NH} + b] \quad (2)$$

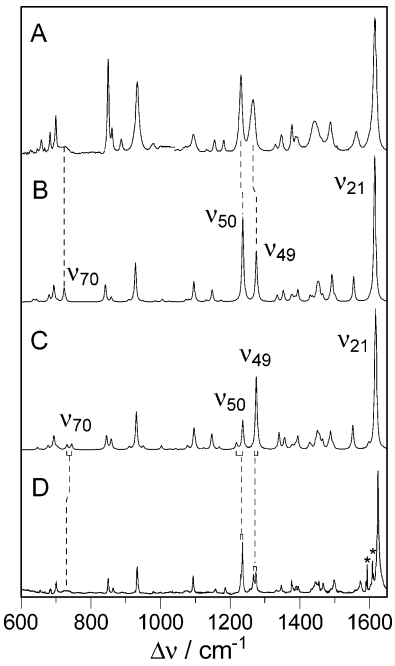

Figure 3. IR spectra of HMPM-D_0 in the frequency range from 600 to 1650 cm^{-1}: A, experimental spectrum of HMPM monomers (1040−1650 cm^{-1} in CD_2Cl_2; 840−1040 cm^{-1} in CCl_4; 600−840 cm^{-1} in cyclohexane); B, calculated spectrum of monomeric HMPM; C, calculated spectrum of dimeric HMPM; D, experimental spectrum of HMPM dimers in Ar matrix. The bands marked with an asterisk correspond to water.

where ν_0 and ν_{mon} are the N−H stretching frequencies of the reference molecule 2,3,4-trimethylpyrrole and of monomeric HMPM, respectively. The values for parameters a and b are assumed to be the same as those determined for the intermolecular hydrogen bond interactions of pyrrole, i.e., $a = 0.0515 \pm 0.0025$ kJ·mol^{-1}·cm and $b = 7.5 \pm 0.4$ kJ·mol^{-1}.[24] Thus, for a frequency shift $\Delta\nu_{NH}$ of 219 cm^{-1}, a value of $\Delta H^{HB}_{298,mon} = -18.8$ kJ·mol^{-1} is obtained for the intramolecular hydrogen bond of HMPM.

The N···N distance can also be taken as an indication of the strength of hydrogen bonds. So far there is no evidence that HMPM crystallizes as the monomer, but theoretical results indicate a stronger intramolecular hydrogen bond in the monomer than in the dimer since the intramolecular N···N distance is 0.16 Å shorter compared to the dimer.[25] This conclusion is supported by the comparison with the crystal structures of related free base pyrromethenes. In these molecules the intramolecular N···N distances are found to be ca. 0.15 Å shorter than in HMPM crystals.[26,27] Also the two additional intermolecular hydrogen bonds that are formed within the dimeric entity are weaker compared to hydrogen bonds between secondary amines and sp^2 hybridized nitrogen atoms as these systems display distinctly shorter N···N distances (2.96 ± 0.13 Å).[28] Thus, formation of HMPM dimers is determined by the tradeoff of two opposing effects, i.e., the energy gain due to formation of additional albeit relatively weak intermolecular hydrogen bonds and the energy loss due to weakening of the intramolecular hydrogen bonds.

Since even in a nonpolar organic solvent at a concentration of 23 mmol·L^{-1} (see above) no HMPM dimers are found within the limit of the detection (>10%), the dimerization constant must be smaller than 7 mol^{-1}·L and the free energy of dimerization $\Delta G_{298,dim}$ less negative than −5 kJ·mol^{-1}. The situation is different for HMPM in the Ar matrix. In the matrix IR spectra shown in Figures 2 and 3, several of the vibrational

bands are split into two components as it is predicted by DFT calculations for HMPM dimers. A particularly large splitting (19 cm^{-1}) between the conjugate modes of the monomeric entities A and B is calculated for the N−H stretching modes, which is in excellent agreement with the experimentally observed splitting between the band components at 3247 and 3230 cm^{-1}(cf. Figure 2C). In HMPM-ND, this doublet is observed at 2435 and 2422 cm^{-1} (cf. Figure 2D). Note that in the matrix IR spectrum of the deuterated sample, the 3247/3230 cm^{-1} doublet is still present. The residual contribution of nondeuterated HMPM dimers may originate from the re-D/H exchange in the sample chamber due to the presence of traces of water, which are also detectable on the basis of characteristic H_2O (dimer, oligomer) bending modes around 1600 cm^{-1}(cf. Figure 3D). Based on a band fitting analysis of the N−H/N−D stretching region, the degree of deuteration was estimated to be ca. 50%.

To estimate the enthalpy of hydrogen bond formation in the dimer, $\Delta H^{HB}_{298,dim}$, the contributions of the individual hydrogen bonds are assumed to combine additively such that eq 2 leads to

$$\Delta H^{HB}_{298,dim} = -[a\cdot(\nu_0 - \nu^a_{dim}) + b] - [a\cdot(\nu_0 - \nu^b_{dim}) + b] \quad (3)$$

where ν^a_{dim} and ν^b_{dim} are the two N−H stretching frequencies of the dimer at 3247 and 3230 cm^{-1} (Figure 2C). With the N−H stretching frequency of the non-hydrogen-bonded reference molecule of 3490 cm^{-1} (vide supra), one obtains $\Delta H^{HB}_{298,dim}$ of −40.9 kJ·mol^{-1}, corresponding to −20.5 kJ·mol^{-1} per HMPM molecule in the dimer.

The hydrogen bond enthalpy difference between the dimer and two monomers, $\Delta\Delta H_{HB}$, is given by

$$\Delta\Delta H_{HB} = \Delta H^{HB}_{298,dim} - 2\cdot\Delta H^{HB}_{298,mon} \quad (4)$$

Upon inserting eqs 2 and 3 into 4 one obtains

$$\Delta\Delta H_{HB} = a\cdot(\nu^a_{dim} + \nu^b_{dim}) - a\cdot 2\cdot\nu_{mon} \quad (5)$$

The determination of the enthalpy difference according to eq 5, which does not depend on the frequency of the reference molecule, yields a value of −3.3 kJ·mol^{-1} for $\Delta\Delta H_{HB}$. Thus, the hydrogen bond enthalpy of the dimer is only slightly more negative than that for two monomers. The main reason for the relatively low hydrogen bond strength in the dimer as compared to that in the monomer are the geometrical constraints of the HMPM molecule. The second molecule can only bind in a quasi-orthogonal position under widening of the methine bridge angle in both monomeric entities.

The difference in the hydrogen bond strength between HMPM dimer and monomers, $\Delta\Delta H_{HB}$, as determined on the basis of an empirical relationship, can be compared with the dimerization enthalpy of HMPM at 298 K in CCl_4 solution, $\Delta H_{298,dim}$, which can be obtained from quantum mechanical calculations.

Equations 2 and 3 refer to the enthalpy difference between the hydrogen bonded (H_{mon}, H_{dim}) and non-hydrogen-bonded (H_0) states, corresponding to

$$\Delta H^{HB}_{298,mon} = (H_{mon} - H_0)$$

$$\Delta H^{HB}_{298,dim} = (H_{dim} - 2H_0) \quad (6)$$

Insertion of eqs 6 into eq 4 leads to

$$\Delta\Delta H_{HB} = H_{dim} - 2\cdot H_{mon} = \Delta H_{298,dim} \quad (7)$$

To evaluate the dimerization enthalpy, we first estimate the corresponding energy difference $\Delta E_{0,dim}$ at 0 K according to

$$\Delta E_{0,dim} = E_{dim}(G_{dim}) - 2\cdot E_{mon}(G_{mon}) + 2\cdot\Delta_{BSSE} \quad (8)$$

where $E_{dim}(G_{dim})$ and $E_{mon}(G_{mon})$ are the energies of the geometry-optimized HMPM dimer and monomer, respectively, and Δ_{BSSE} is a correction term that accounts for the basis set superposition error (BSSE). This error is inevitable in the supermolecule approach if the energy of the monomers is calculated with a smaller basis set than that of the dimer. According to the function counterpoise method,[29] Δ_{BSSE} is given by the energy of the geometry-optimized monomer calculated using the monomer basis set minus the energy of the monomer in the dimer geometry calculated using the full dimer basis set (for a critical review on BSSE corrections, see refs 30 and 31). At the B3LYP/6-31G* level of theory, the uncorrected energy difference $E_{dim}(G_{dim}) - 2E_{mon}(G_{mon})$ is calculated to be −20.4 kJ·mol^{-1}, while a value of +5.8 kJ·mol^{-1} is obtained for Δ_{BSSE}, such that $\Delta E_{0,dim}$ amounts to −8.8 kJ·mol^{-1}.

The conversion of the computed energy difference $\Delta E_{0,dim}$ to the enthalpy difference requires corrections that take into account the differences of the thermal contributions ΔH^{th}_{298} and of the solvation energy in CCl_4 (ΔE_{solv}) according to

$$\Delta H_{298,dim} = \Delta E_{0,dim} + \Delta H^{th}_{298} + \Delta E_{solv} \quad (9)$$

Unscaled B3LYP/6-31G* harmonic vibrational frequency calculations were used to obtain thermal enthalpy corrections at 298 K for HMPM monomer and for HMPM dimer.[32] The difference between these correction terms leads to a value of +6.8 kJ·mol^{-1} for ΔH^{th}_{298}. A rough estimate for ΔE_{solv} is derived from the isodensity polarized continuum model, in which the shape of the cavity of the solute is calculated from the surface for a fixed electron density value and the electrostatic solute−solvent interaction is taken into account to infinite order.[33] Taking an isodensity value of 0.0002 atomic units and a dielectric constant $\epsilon = 2.228$ for CCl_4, a value of +3.3 kJ·mol^{-1} is calculated for ΔE_{solv}. Thus, solvation in a nonpolar solvent energetically favors the monomers over the dimer. This is due to the about 25% larger solvent accessible surface of the prolate-shaped monomers compared to that of the spheroidally shaped dimer which allows for better solute−solvent interaction. With these corrections, a value of +1.3 kJ·mol^{-1} is obtained for $\Delta H_{298,dim}$. The comparison with the experimentally determined enthalpy difference of hydrogen bond formation of −3.3 kJ·mol^{-1} reveals a good agreement, which is in contrast to the previously reported deficiencies of B3LYP/6-31G* calculations to reproduce faithfully the energetics of hydrogen bonding systems.[8]

Since in solution the dimerization entropy is negative, $\Delta\Delta G^{HB}_{298}$ will be more positive such that the failure to detect HMPM dimers in organic solvents can readily be understood. Conversely, the weight of the entropic term is likely to be small in the crystalline state, and in this case formation of dimers is controlled by the negative dimerization enthalpy. These considerations may also hold for HMPM in the Ar matrix, where HMPM dimers prevail. Due to their spheroidal shape, dimers of HMPM have a strong tendency to sublime. At the relatively low heating temperature (ca. 70−80 °C), the crystal structure

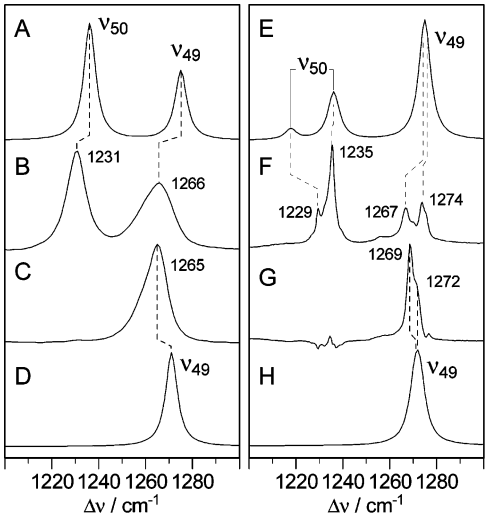

Figure 4. Experimental and calculated IR spectra of HMPM monomers and dimers in the frequency range from 1200 to 1300 cm^{-1}: A, HMPM-D_0 monomer, calculated; B, HMPM-D_0 monomer, experimental; C, HMPM-ND monomer, experimental; B and C measured in CD_2Cl_2 solution; D, HMPM-ND monomer, calculated; E, HMPM-D_0 dimer, calculated; F, HMPM-D_0 dimer, experimental; G, HMPM-ND dimer, experimental; F and G measured in Ar matrix; H, HMPM-ND dimer, calculated.

may be broken without destroying the intermolecular bonds of the HMPM dimers.

(3) Vibrational Analysis of HMPM Dimers. Since the structural differences between HMPM monomers and dimers are predicted to be relatively small and only restricted to a few parameters, the vibrational spectra are expected to be quite similar with respect to frequencies and relative intensities. Inspection of the matrix IR spectra confirms this expectation (cf. Figure 3A,D). Indeed, the mode splitting only exceeds 1 cm^{-1} for those modes including internal coordinates that are altered upon dimerization. Nevertheless, the centers of gravity of the conjugate bands for some of the modes differ by up to 10 cm^{-1} upon dimerization (e.g., ν_{21} and ν_{49}). In the spectra of solid HMPM in KBr pellets, the bands are distinctly broader than in the Ar matrix in such a way that the splitting of modes due to dimer formation is only detectable in a few cases. One example is the band observed at 1257 cm^{-1}, which exhibits a shoulder at 1264 cm^{-1} (cf. Figure 10B). The separation of the two band components is 7 cm^{-1} and thus identical to that of the doublet at 1267 and 1274 cm^{-1} in the Ar matrix spectrum (ν_{49}), but the center of gravity differs by ca. 10 cm^{-1} (cf. Figure 4F). A possible origin of these shifts may lie in the different molecular environment in the Ar matrix and in the solid state. However, IR spectra measured in CD_2Cl_2, CCl_4, and cyclohexane solutions do not reveal a distinct solvent-sensitivity.

Since significant structural differences between HMPM monomers and dimers are restricted to the N···H−N entity and the methine bridge, dimerization-induced spectral differences are mainly expected for modes that involve the N−H and methine bridge coordinates.

N−H Stretching and Deformation Modes. The most pronounced spectral differences occur for the N−H stretching modes (Table 2). For the monomeric form, the frequencies at 3271 (HMPM-D_0) and 2439 cm^{-1} (HMPM-ND) are satisfactorily reproduced by calculations employing the standard scaling factor of 0.9153 and the anharmonicity correction factor of 1.0214.[7] With this scaling factor, which is generally applicable for C−H stretchings as well as for N−H stretchings of non-hydrogen-bonded systems, the differences between calculated and experimental frequencies are 29 and 16 cm^{-1}. A further improvement is achieved by employing a slightly smaller scaling factor (0.90), which reduces the deviations from the experimental values to 1 and 4 cm^{-1}.

This scaling factor, however, is not adequate to reproduce the N−H stretchings of the dimer at 3247 and 3230 cm^{-1} (Table 2). Although the calculated splitting (19 cm^{-1}) agrees well with the experimental finding (17 cm^{-1}), the calculated frequencies are higher by 66 cm^{-1}. Similar results are obtained for the doublet at 2435 and 2422 cm^{-1} in the matrix IR spectrum of HMPM-ND dimer. These findings imply that the hydrogen bond interactions in dimeric HMPM require an adjustment of the scaling factor for the stretching coordinate. In this case, a value of 0.87 provides an adequate correction for the N−H stretching and, upon including the anharmonicity factor, for the N−D stretching mode of HMPM-ND dimer as well.

In contrast to the N−H/N−D stretching, the N−H in-plane (NH ip) deformation coordinate contributes to more than one mode. The largest NH ip contribution is calculated for the mode ν_{50} (48%), which has previously been assigned to an apparent shoulder at ca. 1254 cm^{-1} of the prominent 1266 cm^{-1} band in the RR spectrum of HMPM monomers.[4] This assignment has to be revised in the light of the present IR spectrum, which displays a strong band at 1231 cm^{-1} in CD_2Cl_2 solution (Figure 4B). This band disappears in the spectrum of the HMPM-ND monomer (Figure 4C). The calculated frequency of 1236 cm^{-1} is in good agreement with the experimental value. In the HMPM-ND monomer, mode ν_{60} (1040 cm^{-1}) and the two adjacent modes ν_{65} (929 cm^{-1}) and ν_{66} (927 cm^{-1}) include between 16 and 9% of the ND ip coordinate and are readily assigned to the band at 1039 cm^{-1} and the composite band at ca. 930 cm^{-1}, respectively (Figure 5C,D). The largest ND ip contribution is predicted for the mode ν_{69} at 794 cm^{-1} (31%) for which only a weak IR intensity is calculated. The experimental spectrum displays a broad hump centered at ca. 810 cm^{-1} that is not present in the spectrum of HMPM-D_0 and thus can be assigned to this mode (Figure 6C,D).

The modes of the monomer were calculated with a NH/ND ip scaling factor of 0.91, which provides a good reproduction of all modes including these internal coordinates. If the same factor is used for the dimer, the NH/ND ip coordinates contribute to the same modes (with comparable potential energy distribution (PED)) as in the monomer which are predicted to exhibit substantial splittings, in particular the mode ν_{50} of the nondeuterated HMPM dimer (Figure 4E,F). Also in this case, the assignment is straightforward since there are two distinct bands at 1235 and 1229 cm^{-1}, although the observed splitting is lower than the calculated one (6 cm^{-1} versus 18 cm^{-1}). As shown in Figure 7, no significant improvement in the reproduction of the matrix IR spectrum is achieved when the original scaling factor of 0.91 is altered. An increase of the scaling factors has only a small effect on the splitting but causes frequency upshifts of both bands. Also, in the HMPM-ND dimer the NH ip scaling factor of the monomeric HMPM provides a satisfactory description for the vibrational spectrum of the HMPM dimer (Figure 5G,H).

In the monomeric HMPM-D_0 the NH oop coordinate is largely concentrated in the mode ν_{70} (62%), which is calculated to occur between 700 and 780 cm^{-1} when the NH oop scaling factor is varied between 0.8 and 1.0. The experimental IR spectrum displays a broad band at ca. 725 cm^{-1} which upon H/D exchange is replaced by a comparable broad band at ca.

TABLE 2: Calculated and Experimental Frequencies of the Modes Involving NH and ND Coordinates in HMPM-D_0 and HMPM-ND Monomers and Dimers[a]

monomer				dimer		
mode no.	PED (%)	calcd ν	exptl ν[b]	PED (%)	calcd ν	exptl ν[c]
1	NH str (99)	3272	3271	NH str (99)	3257	3247
				NH str (99)	3238	3230
27	NH ip (7)	1465	–	NH ip (6)	1465	1467
				NH ip (8)	1465	
49	NH ip (6)	1275	1266	NH ip (5)	1275	1274
				NH ip (2)	1275	1267
50	NH ip (48)	1236	1232	NH ip (50)	1236	1235
				NH ip (46)	1218	1229
70	NH oop (62)	724	~725 br[d]	NH oop (74)	745	741[e]
				NH oop (49)	732	727[e]
72	NH oop (13)	703	–	NH oop (13)	703	–
74	NH oop (2)	686	–	NH oop (15)	687	–
				NH oop (10)		682
78	NH oop (24)	636	632	NH oop (39)	643	633[e]
20	ND str (97)	2435	~2439	ND str (97)	2424	2435
				ND str (97)	2411	2422
60	ND ip (16)	1040	1039	ND ip (14)	1034	
				ND ip (12)	1031	
65	ND ip (15)	929	927	ND ip (15)	935	–
				ND ip (9)	935	
66	ND ip (9)	927	932 sh	ND ip (9)	929	932
				ND ip (14)	924	929
69	ND ip (31)	794	~810 br[d]	ND ip (33)	791	795[f]
				ND ip (37)	783	
81	ND oop (103)	509	~507 br	ND oop (76)	519	541[e]
				ND oop (79)	498	
83	ND oop (9)	460	460	ND oop (7)	464	–

[a] Frequencies (cm^{-1}): br, broad; sh, shoulder; str, stretch; ip, in plane; oop, out-of-plane; PED, potential energy distribution. [b] IR spectra measured in CCl_4 if not stated otherwise. [c] Ar matrix IR spectra if not stated otherwise. [d] IR spectra measured in cyclohexane. [e] KBr IR spectra. [f] Solid Raman spectrum.

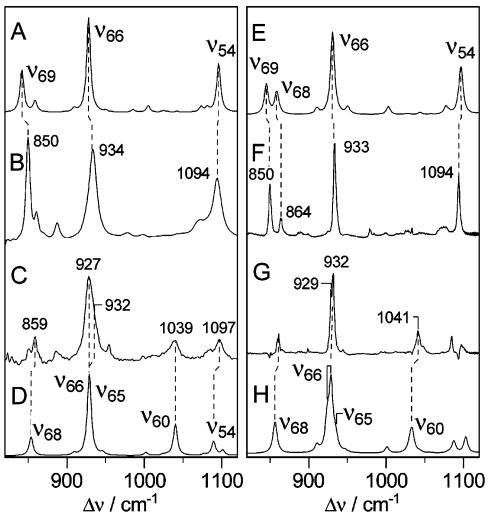

Figure 5. Experimental and calculated IR spectra of HMPM monomers and dimers in the frequency range from 820 to 1120 cm^{-1}: A, HMPM-D_0 monomer, calculated; B, HMPM-D_0 monomer, experimental; C, HMPM-ND monomer, experimental, B and C measured in CCl_4 solution; D, HMPM-ND monomer, calculated; E, HMPM-D_0 dimer, calculated; F, HMPM-D_0 dimer, experimental; G, HMPM-ND dimer, experimental, F and G measured in Ar matrix; H, HMPM-ND dimer, calculated.

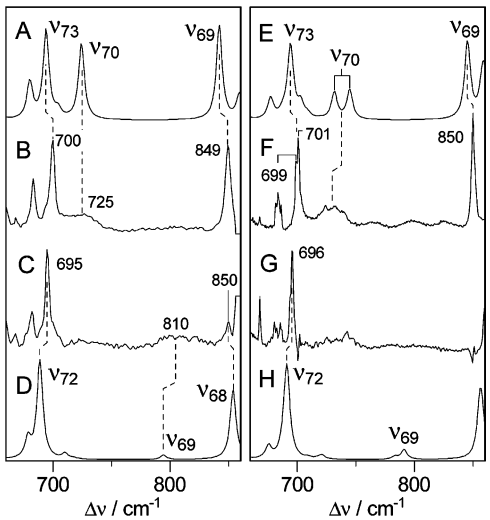

Figure 6. Experimental and calculated IR spectra of HMPM monomers and dimers in the frequency range from 660 to 860 cm^{-1}: A, HMPM-D_0 monomer, calculated; B, HMPM-D_0 monomer, experimental; C, HMPM-ND monomer, experimental, B and C measured in cyclohexane solution; D, HMPM-ND monomer, calculated; E, HMPM-D_0 dimer, calculated; F, HMPM-D_0 dimer, experimental; G, HMPM-ND dimer, experimental, F and G measured in Ar matrix; H, HMPM-ND dimer, calculated.

507 cm^{-1} (cf. Figures 6B and 8B). The best reproduction of the experimental bands is achieved with a NH oop scaling factor of 0.85.

Since the frequency region below 600 cm^{-1} was not accessible in the Ar matrix IR experiments, we have analyzed the ND as well as the NH oop modes of HMPM dimers on the basis of the IR spectra obtained from solid HMPM in KBr pellets. For HMPM-D_0 dimers, two broad bands at 741 and 727 cm^{-1} are clearly identified (Figure 9) and can be assigned to the NH oop modes since they are replaced by a band at 541 cm^{-1} in HMPM-ND (data not shown). Using the same value of the scaling factor as for the NH oop coordinate of monomeric HMPM, i.e., 0.85, the NH oop modes are calculated at 715 and 816 cm^{-1}, which is in distinct contradiction with the experimental findings. Neither larger nor smaller scaling factors improve the agreement with the experimental data, as can be

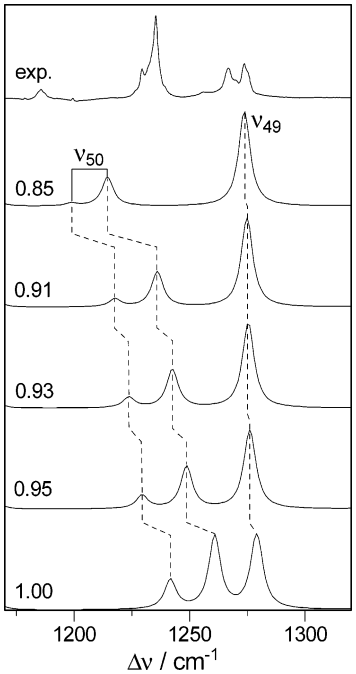

Figure 7. Experimental IR spectrum of HMPM-D_0 dimers in the Ar matrix in the frequency range between 1170 and 1320 cm^{-1} (top) compared with the calculated IR spectra obtained with different NH ip scaling factors.

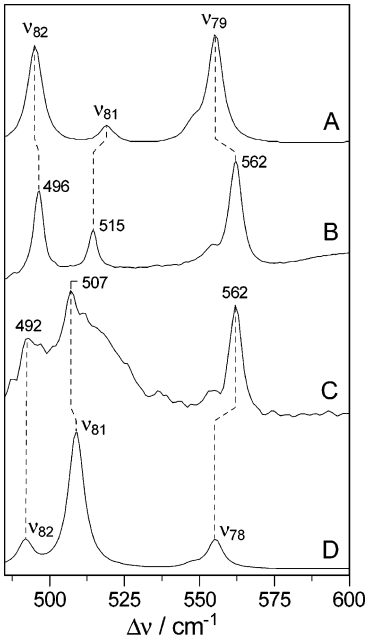

Figure 8. Calculated and experimental IR spectrum of monomeric HMPM in the frequency range between 485 and 600 cm^{-1}: A, HMPM-D_0 monomer, calculated; B, HMPM-D_0 monomer, experimental; C, HMPM-ND monomer, experimental, B and C measured in CCl_4 solution; D, HMPM-ND monomer, calculated.

seen in Figure 9. In the former case ($\sigma_{\mathrm{NH\ oop}} = 0.92$), the two calculated modes shift up to 736 and 846 cm^{-1} which, hence, cannot account for the observed two-banded structure at 727 and 741 cm^{-1} in the experimental spectrum. Moreover, in HMPM-ND only the lower frequency mode (510 cm^{-1}) is in acceptable agreement with the observed band at 541 cm^{-1}, whereas for the second mode, which is calculated to occur at 603 cm^{-1} with a considerable IR intensity, no counterpart is observed in the experimental spectrum. On the other hand, a lower scaling factor than 0.85 (i.e., $\sigma_{\mathrm{NH\ oop}} = 0.75$), also does

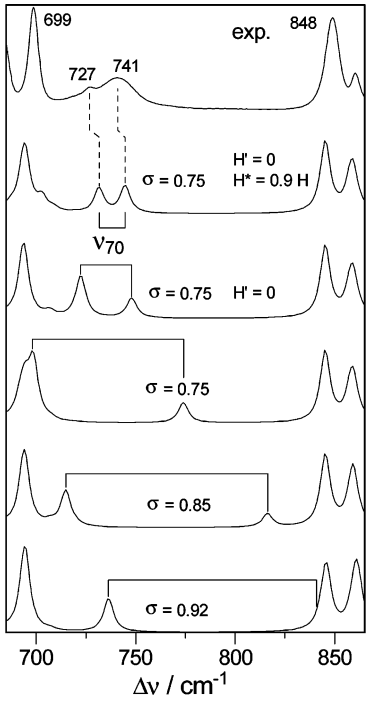

Figure 9. Experimental IR spectrum of HMPM-D_0 dimers in KBr pellets in the frequency range between 685 and 870 cm^{-1} (top) compared with the calculated IR spectra obtained with different NH oop scaling factors and coupling constants H' and H^*.

not provide a good description of the experimental spectrum. In this case, the two NH oop modes are calculated to occur at 669 and 774 cm^{-1}. Although the mean frequency is about the same as the mean frequency of the experimentally observed band pair, the calculated splitting is much higher (75 cm^{-1}) than in the experimental spectrum (14 cm^{-1}). It appears therefore that a satisfactory reproduction of the experimental spectrum is not possible solely by adjusting the scaling factor. This conclusion thus points to a failure of the B3LYP/ 6-31G* approximation for calculating vibrational spectra of this hydrogen bonded system.

The factors that control the splitting of the NH oop modes are the interaction constant H' of the NH oop coordinates of the two HMPM molecules and the coupling constants of the NH oop and other internal coordinates. Upon setting H' equal to zero, the splitting is largely reduced. However, the intensity ratio of both modes is reversed compared to the experimental bands at 741 and 727 cm^{-1}. Furthermore, a close inspection of the mode composition reveals a substantial coupling of the NH oop with the pyrrole torsion* coordinate (for the definition of internal coordinates see ref 34). This torsional coordinate is involved in various modes of the dimer that exhibit a surprisingly large splitting. If the coupling constant H^* between these coordinates is reduced by 10%, good agreement with the experimental spectra is achieved. Note that this parametrization leaves the other modes virtually unchanged, and thus it represents a selective correction for the NH oop modes.

Vibrations Involving the Methine C−H Group. To identify the modes that involve the methine bridge coordinates, we analyzed the IR spectra of HMPM-D_0 and HMPM-CD dimers measured in KBr pellets. In the system of natural internal coordinates,[34] the methine group is involved in six internal coordinates. These are the methine CH stretching, the methine CH rocking, the methine angle deformation, the CH oop coordinate, and the methine C−C and C═C torsional coordinates. Among them, the methine CH stretching coordinate is

TABLE 3: Calculated and Experimental Frequencies of the Modes Involving CH and CD Coordinates of the Methine Bridge in HMPM-D_0 and HMPM-CD Monomers and Dimers[a]

monomer				dimer		
mode no.	PED (%)	calcd ν	exptl ν[b]	PED (%)	calcd ν	exptl ν[c]
2	CH str (100)	3055	~3041[d]	CH str (99)	3052	3045
				CH str (99)	3052	
21	C═C str (38) CH rock(11)	1615	1616	C═C str (41) CH rock (13)	1618	1610
				C═C str (41) CH rock (13)	1616	
47	CH rock(12)	1352	1345	CH rock (27)[e]	1358	1343
				CH rock (29)[e]	1357	
48	CH rock (21)	1335	1329	CH rock (10)	1341	1327
				CH rock (9)	1340	
49	CH rock (17)	1275	1265	CH rock(14)	1275	1264 sh, 1257
				CH rock (15)	1275	
67	CH oop (77)	909	888	CH oop (77)	911	887
				CH oop (77)	911	
68	methine angle def (12)	859	861	methine angle def (10)	860	861
				methine angle def (9)	858	
69	methine angle def (2)	842	850	methine angle def (5)	845	849
				methine angle def (7)	845	
83	methine C═C tors (15)	462	462	methine C═C tors (18)	467	466
				methine C═C tors (16)	465	
20	CD str (98)	2277	2261[d]	CD str (98)	2273	2256
				CD str (98)	2273	
21	C═C str (16)	1605	1603[d]	C═C str (38)	1604	1598
				C═C str (37)	1602	
64	CD rock (19)	961	955[f]	CD rock (25)	965	955
				CD rock (26)	965	
66	CD ip (18)	914	916[d]	CD rock (14)	921	912
				CD rock (14)	920	
67	methine angle def (13)	847	849[d]	methine angle def (12)	847	849
				methine angle def (12)	846	
68	CD rock (13)	820	829[d]	CD rock (13)	822	829
				CD rock (13)	821	
69	CD oop (61)	771	759[d]	CD oop (53)	773	756
				CD oop (64)	770	
83	methine C═C tors (19)	442	–	methine C═C tors (22)	445	445
				methine C═C tors (20)	444	

[a] Frequencies (cm^{-1}): sh, shoulder; str, stretch; rock, rocking; oop, out-of-plane; def, deformation; tors, torsion. [b] IR spectrum measured in CCl_4 if not stated otherwise. [c] KBr IR spectra. [d] IR spectrum measured in CD_2Cl_2. [e] Mode number 46 in the dimer. [f] IR spectrum measured in cyclohexane.

specific inasmuch as it does not couple to any significant extent with the other internal coordinates of the dimer (Table 3). This mode ν_2 (3052 cm^{-1}) is well-separated from the other CH stretchings in HMPM-D_0 and calculated at 2273 cm^{-1} for HMPM-CD with an almost unchanged mode composition. This methine CH stretching mode can be easily identified in the experimental spectra of HMPM-D_0 and HMPM-CD at 3045 and 2256 cm^{-1}, respectively (data not shown).

Deuteration at the methine bridge causes drastic alterations of band pattern in the entire frequency range between 600 and 1300 cm^{-1}. The CH rocking coordinate is predicted to contribute with more than 10% to the PED of four modes, ν_{21}, ν_{46}, ν_{48}, and ν_{49} in HMPM-D_0. Mode ν_{21}, which predominantly involves the C═C stretching of the methine bridge, is predicted to be the strongest band in the IR spectrum in agreement with the experiment. In HMPM-CD, the frequency is calculated to shift from 1617 to 1603 cm^{-1} upon methine deuteration, which compares well with the experimentally observed downshift of 12 cm^{-1} (Table 3). The largest CH rocking contribution (29%) is calculated for ν_{46} at 1357 cm^{-1}, which is in close vicinity of ν_{47} and ν_{48} (1356 and 1340 cm^{-1}). Upon H/D substitution at the methine bridge, frequencies and relative intensities of the latter two modes remain largely unchanged, whereas the counterpart of the mode ν_{46} (26% CD rock) shifts down to 965 cm^{-1}. Since the intensity of ν_{46} is calculated to be smaller by a factor of 6 compared to the sum of the intensities of ν_{47} and ν_{48}, the intensity in this region should not be significantly altered upon methine-bridge deuteration, which is in fact confirmed by the experimental spectra (Figure 10B,C). Also the CD rocking mode ν_{64} can readily be assigned to a band at 955 cm^{-1}, which is in good agreement with the calculated frequency (cf. Table 3 and Figure 11C, D). The mode ν_{49}, calculated at 1275 cm^{-1}, involves a large number of internal coordinates of relatively small weight, among which the largest contribution (14%) is provided by the CH rocking. In HMPM-CD, the composition is substantially redistributed, leading to three modes in this region (1303, 1180, and 1158 cm^{-1}), which all are predicted to exhibit considerable IR intensity. In view of the good agreement in frequencies and relative intensities, these modes can be assigned to the bands at 1294, 1198, and 1165 cm^{-1} in the experimental IR spectrum of HMPM-CD (Figure 10C,D). The nearby NH deformation mode ν_{50} is also strongly affected in HMPM-D_0 by methine bridge deuteration. A significant upshift from 1236 to 1245 cm^{-1} and a strong reduction of the IR intensity is predicted for ν_{50}, although the weight of the CH rocking coordinate is only very low. Again, we note a good agreement with the experimental spectrum of HMPM-CD, which displays a band at 1238 cm^{-1} that is much weaker and upshifted by 9 cm^{-1} compared to the corresponding band in HMPM-D_0 (Figure 10B,C). In contrast, the calculations fail to reproduce the experimental intensity ratio of modes ν_{49} and ν_{50} in HMPM-D_0 in which the CH rocking and the NH deformation coordinates are strongly coupled.

In the calculated vibrational spectrum of HMPM-D_0, the CH oop coordinate is largely localized in the mode ν_{67} (77%) at 911 cm^{-1}. It can be assigned to the band at 887 cm^{-1} of HMPM-

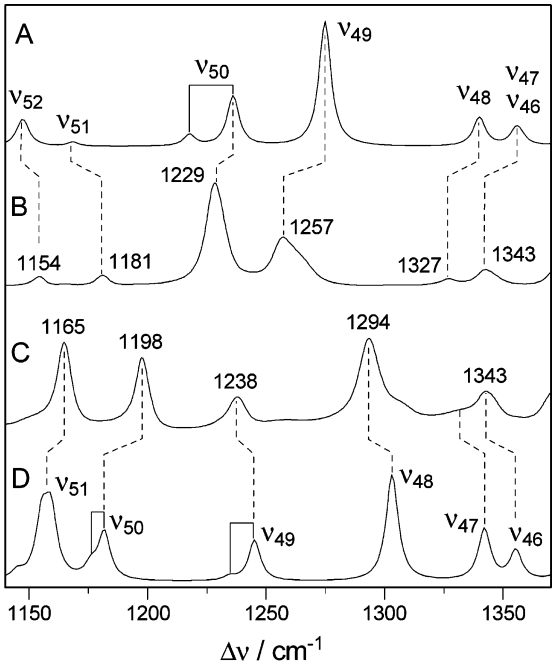

Figure 10. Calculated and experimental IR spectra of dimeric HMPM in KBr pellets in the frequency range between 1140 and 1370 cm^{-1}: A, HMPM-D_0, calculated; B, HMPM-D_0, experimental; C, HMPM-CD, experimental; D, HMPM-CD, calculated.

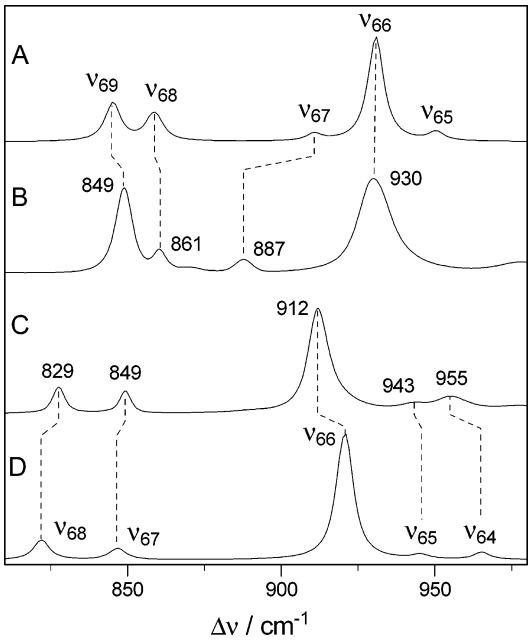

Figure 11. Calculated and experimental IR spectra of dimeric HMPM in KBr pellets in the frequency range between 810 and 975 cm^{-1}: A, HMPM-D_0, calculated; B, HMPM-D_0, experimental; C, HMPM-CD, experimental; D, HMPM-CD, calculated.

D_0 (Figure 11A,B), which disappears upon methine bridge deuteration and the corresponding CD oop band is found at 756 cm^{-1} in good agreement with the calculations (773 cm^{-1}; data not shown).

The methine angle deformation coordinate in HMPM-D_0 is calculated to contribute to two modes (ν_{68} and ν_{69}) of significant IR intensity. These modes include a complex superposition of stretches of the pyrrolic and pyrroleninic C−C and N−C bonds, which all contribute with small weights. Although the weight of the methine angle deformation is also small, deuterium substitution at the methine bridge is predicted to cause marked frequency downshifts from 859 to 847 cm^{-1} and from 845 to 822 cm^{-1} for ν_{68} and ν_{69}, respectively (Figure 11A,D). In view of the good agreement with the calculated frequencies and intensities, the bands observed at 861 and 849 cm^{-1} in the HMPM-D_0 spectrum can be readily assigned to ν_{68} and ν_{69}, respectively, and the bands observed at 849 and 829 cm^{-1} in HMPM-CD to their counterparts ν_{67} and ν_{68}, respectively (Figure 11). The frequency shifts (ν_{68}[HMPM-D_0]−ν_{67}[HMPM-CD]) and (ν_{69}[HMPM-D_0]−ν_{68}[HMPM-CD]) are 12 and 20 cm^{-1}, respectively, which is also in good accordance with the calculations.

The two methine torsional coordinates are involved in several modes below ca. 900 cm^{-1}, with the largest contribution of the methine C═C torsion to the mode ν_{83}. Also in this case, the predicted shift upon methine bridge deuteration from 465 to 444 cm^{-1} is confirmed by the experimental bands at 466 and 445 cm^{-1} in the spectra of HMPM-D_0 and HMPM-CD, respectively (Table 3).

Inspection of the experimental and calculated IR spectra for the monomeric HMPM-D_0 and HMPM-CD (data not shown) offers the same picture, inasmuch as the spectral changes brought about by methine bridge deuteration are essentially the same as for HMPM dimer. Thus, it appears that the widening of the methine bridge angle in the dimer does not result in significant changes in the vibrational spectra.

Comparison of Various Hydrogen-Bonded Systems. The hydrogen bonded systems studied in this and in our previous work[7] can be ranked with respect to the calculated hydrogen bond strength based on the use of eq 2. It is found that $|\Delta H^{HB}_{298}|$ increases in the order HMPM monomer < maleimide dimer < HMPM dimer < pyrrolidone dimer (Table 4). The scaling factors that have been optimized for the N−H str as well as for the NH ip and NH oop coordinates of the individual systems do not vary in the same order. Thus, there is no indication that the error associated with the DFT calculation per se scales with the predicted strength of the hydrogen bond. Evidently, these errors are also not correlated with the calculated geometries, which were shown to reproduce the experimental data very well.[7,36,38] The variations of the scaling factors for the three coordinates do not exhibit a common tendency. Thus, one has to conclude that at present, i.e., on the basis of the yet rather small data set, it is not possible to predict appropriate scaling factors for these coordinates in different hydrogen bond systems. It is worth noting that for the limiting case of a non-hydrogen-bonded N−H group, i.e, for monomeric maleimide and pyrrolidone, the scaling factor of each coordinate is closer to unity than for the other cases. This finding further supports the conclusion that the problems associated with reproducing the frequencies of the NH-containing modes are solely related to the deficiencies of the B3LYP/6-31G* approximation to give the force constants of the hydrogen bonded N−H group. Thus, scaling factors for hydrogen bonded N−H groups have to be adjusted for the individual systems and consequently might only be transferable between chemically and structurally related molecules. In the case of the NH oop modes of the HMPM and pyrrolidone dimers, satisfactory reproduction of the experimental data cannot be achieved solely by varying the scaling factor but requires further adjustments of interaction matrix elements. In contrast to monomeric HMPM and maleimide dimers, the hydrogen bond geometries exhibit out-of-plane distortions in the case of pyrrolidone dimers and particularly of HMPM dimers, in which the hydrogen atoms of the two bifurcated

TABLE 4: Hydrogen Bond Strengths and Scaling Factors for the NH Coordinates of Different Hydrogen Bonded Systems

	maleimide monomer	pyrrolidone monomer	HMPM monomer	maleimide dimer	HMPM dimer	pyrrolidone dimer
type of hydrogen bond	no	no	intramolecular	intermolecular	intra- and intermolecular	intermolecular
ν_{NH} (cm^{-1})	3486[a]	3478[b]	3271[c]	3255[a]	3239[c]	3172[d]
ΔH^{HB}_{298} ($kJ \cdot mol^{-1}$)	−	−	-18.8	−19.4	−20.5	−23.3[e]
			Scaling Factor			
NH str	0.9153	0.9153	0.90	0.91	0.87	0.91
NH ip	0.9693	0.9693	0.91	0.89	0.91	0.89
NH oop	1.0120	1.0120	0.85	0.83	0.75[f]	0.87[f]

[a] Ar matrix IR data from ref 35. [b] Ar matrix IR data from ref 36. [c] This work (mean value). [d] Solid IR data from ref 36. [e] A value of −16 $kJ \cdot mol^{-1}$ has been determined from the temperature dependence of the dimerization constant in CCl_4 solution.[37] [f] In addition to scaling, the force constant matrix element for the intermolecular NH oop interaction was modified.

hydrogen bond systems are approximately located on two triangular sides of the tetrahedron made up by the four nitrogen atoms.

The intrinsic deficiencies of the B3LYP method, however, may only have a relatively small impact on the RR spectroscopic analysis of tetrapyrrole chromophores. Experimental RR spectra, particularly of protein-bound chromophores, are generally confined to the region below 1700 cm^{-1} since NH stretchings exhibit only a very low RR intensity. In contrast to the NH str coordinate, the NH ip coordinate is distributed among various modes. Many of these modes exhibit a relatively high RR intensity due to the involvement of coordinates that are associated with large excited-state displacements. However, in each of these modes the relative contribution of the NH ip coordinate is relatively small such that the sensitivity of the calculated frequencies on the NH ip scaling factor is relatively low. This has been confirmed by the spectrum calculated for the *ZZZasa* conformation of the protonated phycocyanobilin.[39] In this case, the standard scaling factor optimized for non-hydrogen-bonded systems provides a satisfactory reproduction of the experimental spectra in the range between 1200 and 1600 cm^{-1}, including the modes that involve the NH ip coordinates from four different N−H groups. Whereas for these modes also a fine-tuning of the NH ip scaling factor is possible on the basis of the experimental bands and the H/D isotope effects, the modes including the N−H oop coordinates remain largely invisible in the RR spectrum. Thus, inappropriate choice of the NH oop scaling factor may indirectly affect the RR spectrum via a redistribution of the PED and concomitant frequency and intensity changes of modes in the vicinity of NH oop modes.

Conclusions

(1) We have shown that HMPM is a monomer in cyclohexane, CCl_4, and CD_2Cl_2 (concentrations, ∼2−23 $mmol \cdot L^{-1}$) but a dimer in the solid. The geometry of the dimer is well-reproduced by B3LYP/6-31G* theoretical calculations, which have also been used to calculate the structure of the monomer. A comparison of the calculated structures of HMPM in the monomer and dimer reveals only small geometry changes on dimerization, mainly in the N−H···N entity and the methine bridge.

(2) The calculations show dimerization of HMPM weakens the intramolecular hydrogen-bond between the pyrrolic and pyrroleninic rings, due to the formation of intermolecular hydrogen bonds and the concomitant widening of the methine bridge angles. Moreover, it is shown that the dimerization constant in organic nonpolar solvents is too low for an appreciable population of dimers to be observed, even at high total HMPM concentrations, and this is confirmed by experiment.

(3) The experimental Ar matrix IR spectra of HMPM dimers reveal a splitting of the vibrational modes compared to the experimental solution IR spectra, particularly for the modes involving the N−H coordinates, and this is predicted by the calculations. Reproduction of these modes in the calculations requires specific adjustments of the NH scaling factors for both monomeric and the dimeric HMPM. In the case of the NH oop coordinate of HMPM dimers, additional corrections of intra- and intermolecular coupling constants in the force field are necessary, but other calculated modes remain unaffected.

(4) The modes involving the methine bridge coordinates do not differ substantially in the spectra of the HMPM monomers and dimers. H/D substitution at the methine bridge leads to a decoupling of the CH and NH ip and oop coordinates, which strongly facilitates the vibrational assignment. Such isotopic labeling should be useful for the interpretion of the vibrational spectra of tetrapyrroles, since CH oop modes constitute important marker bands for the chromophore structure.

Acknowledgment. We gratefully acknowledge the skillful measurements of IR spectra and Ar matrix IR spectra by Mrs. Dagmar Merkel and Mr. Axel Martin. The work was supported by the DFG (SFB 498).

Supporting Information Available: Tables of X-ray data collection information, atom coordinates and thermal parameters, and bond lengths and angles, together with CIF data for HMPM; calculated harmonic vibrational frequencies, IR and Raman intensities (HMPM monomer and dimer), and PED contributions (HMPM dimer); experimental frequencies and intensities of IR spectra (Ar matrix, KBr pellets, in CCl_4, CD_2Cl_2, and cyclohexane solutions) and of Raman spectra (solid); Table 5 of HMPM-D_0 data and Table 6 of HMPM-ND data; experimental frequencies and intensities of IR spectra (KBr pellets and in CD_2Cl_2 and cyclohexane solutions) of HMPM-CD (Table 7); and experimental frequencies and intensities of IR spectra (in CD_2Cl_2 and cyclohexane solutions) of HMPM-CD-ND (Table 8) (pdf). This material is available free of charge via the Internet at http://pubs.acs.org.

References and Notes

(1) Gärtner, W.; Braslavsky, S. E. The phytochromes: spectroscopy and function. In *Photoreceptors and Light Signaling*; Batschauer, A., Ed.; Comprehensive Series in Photochemistry & Photobiology, Vol. 3; The Royal Society of Chemistry: London, 2003; pp 136−180.

(2) Sineshchekov, V. A. *Photochem. Photobiol. Sci*. **2004**, *3*, 596.

(3) Quail, P. H. *Nat. Rev.* **2002**, *3*, 85.

(4) Mroginski, M.-A.; Németh, K.; Magdó, I.; Müller, M.; Robben, U.; Della Védova, C.; Hildebrandt, P.; Mark, F. *J. Phys. Chem. B* **2000**, *104*, 10885.

(5) Rüdiger, W.; Brandlmeier, T.; Blos, I.; Gossauer, A.; Weller, J.-P. *Z. Naturforsch*. **1980**, *35c*, 763.

(6) Rüdiger, W.; Thümmler, F. The phytochrome chromophore. In *Photomorphogenesis in Plants*, 2nd ed.; Kendrick, R. E., Kronenberg, G. H. M., Eds.: Kluwer: Dordrecht, The Netherlands, 1993; pp 51−69.
(7) Magdó, I.; Németh, K.; Mark, F.; Hildebrandt, P.; Schaffner, K. *J. Phys. Chem. A* **1999**, *103*, 289.
(8) Del Bene, J. E.; Person, W. B.; Szczepaniak, K. *J. Phys. Chem.* **1995**, *99*, 10705.
(9) For the nomenclature see: Fischer, H.; Orth, H. *Die Chemie des Pyrrols*, Vol. I; Johnson Reprint: New York, 1968; p 18.
(10) Badger, G. M.; Harris, R. L. N.; Jones, R. A.; *Aust. J. Chem.* **1964**, *17*, 1013.
(11) Fischer, H.; Friedrich, H.; Lamatsch, W.; Morgenroth, K. *Ann. Chem.* **1928**, *466*, 147.
(12) Sheldrick, G. M. *SHELX-97. Program for structure solution and refinement*; University of Göttingen: Göttingen, Germany, 1997.
(13) Klotzbücher, W. E. *Cryogenics* **1983**, 23, 554.
(14) Gerhartz, W.; Grevels, F.-W.; Klotzbücher, W. E. *Organometallics* **1987**, *6*, 1850.
(15) Becke, A. D. *J. Chem. Phys.* **1993**, *98*, 5648.
(16) (a) Hehre, W. J.; Ditchfield, R.; Pople, J. A. *J. Chem. Phys.* **1972**, *56*, 2257. (b) Hariharan, P. C.; Pople, J. A. *Theor. Chim. Acta* **1973**, *28*, 213.
(17) Pulay, P.; Fogarasi, G.; Pongor, G.; Boggs, J. E.; Vargha, A. *J. Am. Chem. Soc*. **1983**, *105*, 7037.
(18) Jeffrey, G. A.; Saenger, W. *Hydrogen Bonding in Biological Structures*; Springer-Verlag: Berlin, 1991; pp 136 ff.
(19) Ma, B.; Lii, J. H.; Schaefer, H. F., III; Allinger, N. L. *J. Phys. Chem*. **1996**, *100*, 8763.
(20) Badger, G. M.; Harris, R. L. N.; Jones, R. A.; Sasse, J. M. *J. Chem. Soc*. **1962**, 4329.
(21) Guy, R. W.; Jones, R. A. *Aust. J. Chem*. **1966**, *19*, 1871.
(22) Abraham, R. J.; Bullock, E.; Mitra, S. S. *Can. J. Chem.* **1959**, *37*, 1859.
(23) Falk, H.; Gergely, S.; Hofer, O. *Monatsh. Chem.* **1974**, *105*, 853.
(24) Nozari, M. S.; Drago, R. S. *J. Am. Chem. Soc*. **1970**, *92*, 7086.
(25) Calculated structural data for the monomer are reported in ref 4.
(26) Sheldrick, W. S.; Borkenstein, A.; Struckmeier, G.; Engel, J. *Acta Crystallogr. B* **1978**, *34*, 329.
(27) Dattagupta, J. K.; Meyer, E. F., Jr.; Cullen, D. L.; Falk, H.; Gergely, S. *Acta Crystallogr., Sect. C: Cryst. Struct. Commun.* **1983**, *39*, 1384.
(28) Gavezzotti, A.; Filippini, G. *J. Phys. Chem.* **1994**, *98*, 4831.
(29) Boys, S. F.; Bernardi, F. *Mol. Phys*. **1970**, *19*, 553.
(30) Gutowski, M.; Chalasiński, G. *J. Chem. Phys*. **1993**, *98*, 5540.
(31) van Duijneveldt, F. B.; van Duijneveldt, J. G. C. M.; van Lenthe, J. H. *Chem. Rev*. **1994**, *94*, 1873.
(32) Ochterski, J. W. *Technical Support Information to Thermochemistry in Gaussian*; Gaussian, Inc.: Pittsburgh, PA, 2000.
(33) Foresman, J. B.; Keith, T. A.; Wiberg, K. B.; Snoonian, J.; Frisch, M. J. *J. Phys. Chem.* **1996**, *100*, 16098.
(34) Pulay, P.; Fogarasi, G.; Pang, F.; Boggs, J. E. *J. Am. Chem. Soc.* **1979**, *101*, 2550.
(35) (a) Barnes, A. J.; Le Gall, L.; Madec, C.; Lauransen, J. *J. Mol. Struct.* **1977**, *38*, 109. (b) Le Gall, L.; Barnes, A. J. *Ber. Bunsen-Ges. Phys. Chem*. **1978**, *82*, 52.
(36) Kneip, C.; Baron, M.-H.; Fillaux, F.; Mark, F.; Hildebrandt, P. Unpublished work
(37) Luck, W. *Naturwissenschaften* **1965**, *52*, 25.
(38) Goddard, R.; Heinemann, O.; Krüger, C.; Magdó, I.; Mark, F.; Schaffner, K. *Acta Crystallogr., Sect. C: Cryst. Struct. Commun.* **1998**, *54*, 501.
(39) Kneip, C.; Hildebrandt, P.; Németh, K.; Mark, F.; Schaffner, K. *Chem. Phys. Lett.* **1999**, *311*, 479.